Taylor & Francis
Taylor & Francis Group

International Journal of Control

ISSN: 0020-7179 (Print) 1366-5820 (Online) Journal homepage: https://www.tandfonline.com/loi/tcon20

A multiobjective H∞ control strategy for energy harvesting in regenerative vehicle suspension systems

Alessandro Casavola, Fabio Di Iorio & Francesco Tedesco

To cite this article: Alessandro Casavola, Fabio Di Iorio & Francesco Tedesco (2018) A multiobjective H∞ control strategy for energy harvesting in regenerative vehicle suspension systems, International Journal of Control, 91:4, 741-754, DOI: 10.1080/00207179.2017.1293298

To link to this article: https://doi.org/10.1080/00207179.2017.1293298

Accepted author version posted online: 08 Feb 2017.
Published online: 22 Feb 2017.

Submit your article to this journal

Article views: 254

View related articles

View Crossmark data

Citing articles: 2 View citing articles

Full Terms & Conditions of access and use can be found at
https://www.tandfonline.com/action/journalInformation?journalCode=tcon20

INTERNATIONAL JOURNAL OF CONTROL, 2018
VOL. 91, NO. 4, 741–754
http://dx.doi.org/10.1080/00207179.2017.1293298

Taylor & Francis
Taylor & Francis Group

A multiobjective $\mathcal{H}_\infty$ control strategy for energy harvesting in regenerative vehicle suspension systems

Alessandro Casavola[a], Fabio Di Iorio[b] and Francesco Tedesco[a]

[a]Dipartimento di Ingegneria Informatica, Modellistica, Elettronica e Sistemistica (DIMES), Università degli Studi della Calabria, Rende, Italy;
[b]McLaren Automotive Ltd, Woking, United Kingdom

ABSTRACT

A significant amount of energy induced by road unevenness and vehicle roll and pitch motions is usually dissipated by conventional shock-absorbers. In this paper, a novel active multiobjective $\mathcal{H}_\infty$ control design methodology is proposed which explicitly includes, besides the usual control objectives on ride comfort, road handling and suspension stroke, the amount of energy to be harvested as an additional, though conflicting, control objective and allows the designer to directly trade-off among them depending on the application. An electromechanical regenerative suspension system is considered where the viscous damper is replaced by a linear electrical motor which is actively governed. It is shown that the proposed control law is able to achieve remarkable improvements on the amount of the harvested energy with respect to passive or semi-active control strategies while maintaining the other objectives at acceptable levels. Simulative studies undertaken via CarSim are also reported that confirm the potentiality and flexibility of the proposed control design strategy.

ARTICLE HISTORY
Received 18 April 2016
Accepted 6 February 2017

KEYWORDS
Energy-harvesting;
suspension systems;
H-infinity control

1. Introduction

In the last decade, the development and the analysis of novel control design methods for active or semi-active suspension systems for automobiles has received a great attention by academic and industrial researchers and many solutions based on different perspectives and approaches are now available (e.g. see Sabzehgar, Maravandi, & Moallem, 2014; Sammier, Sename, & Dugard, 2000 and references therein).

A typical architecture of an active suspension system consists of a spring in parallel with a viscous damper and a force actuator. A related technology is that of *regenerative suspension systems* (Montazeri & Soleymani, 2010), which aim at converting the kinetic and potential energy of the suspensions into electrical energy via an electromechanical generator instead of dissipating it. If such systems did equip a hybrid or electrical vehicle, the harvested energy could be used to recharge the vehicle's battery and hence extend its mileage. In traditional vehicles, the harvested energy could be used to power the electrical subsystems and hence reducing the workload of the internal combustion engine.

Most of the works on regenerative suspension systems (see e.g. Montazeri & Soleymani, 2010; Pires, Smith, Houghton, & McMahon, 2013; Sabzehgar et al., 2014; Sagiv & Bobrovsky, 2011; Scruggs, 2010; Spelta et al., 2010; Zuo, Scully, Shestani, & Zhou, 2010) have been concerned with the technological and constructive details of the electrical motors and drivers and the control design aspects have found less consideration with rare exceptions (see e.g. Scruggs, 2010). In fact, in the literature, the most used control strategy in such a kind of applications is the one which makes the electrical motor behave as a viscous passive damper. A more recent contribution in this respect can be found in Zhang, Cao, and Yu (2012).

The aim of this paper is to propose a novel active multiobjective $\mathcal{H}_\infty$ control design methodology for regenerative vehicle suspension systems which explicitly includes the amount of harvestable energy among the usual control objectives on ride comfort, suspension stroke and road handling to trade-off. In the case of regenerative suspension systems, the presence of conflicting objectives, some to be minimised and some maximised, makes the design problem more difficult, giving rise to possible non-convex optimisation problems when approached directly within the Linear Matrix Inequalities (LMI) optimisation framework.

This difficulty is addressed and solved in this paper by analysing and exploiting the relationship between electrical and mechanical power amounts in the regenerative system, flowing from the road to the electromechanical actuator. It will be shown that the employment of active control strategies in regenerative suspension systems might improve considerably the harvested energy

CONTACT Francesco Tedesco ftedesco@dimes.unical.it

© 2017 Informa UK Limited, trading as Taylor & Francis Group

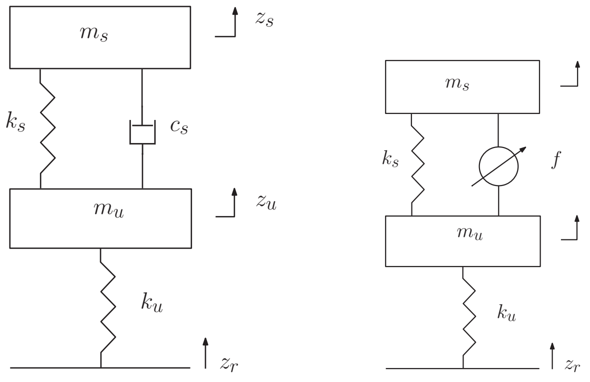

Figure 1. Passive set-up (left)and regenerative set-up (right).

w.r.t. passive or clipped strategies while satisfying, at the same time, the other control specifications.

This paper extends preliminary results given in Di Iorio and Casavola (2012) and Casavola and Di Iorio (2012), where the MIPC control was introduced for the first time. Here, an exhaustive discussion and comparisons with other more traditional control strategies are reported.

1.1 The 2-DOF quarter-car model

The 2-DOF quarter-car model depicted in Figure 1 is used for control design purposes. In the regenerative set-up, the passive viscous damper pertaining to the traditional suspension systems is replaced by an electromechanical actuator that generates a force $f(t)$ to suitably dampen the vertical motion. A classical quarter-car dynamical model for the passive set-up is given by

$$m_s\ddot{z}_s(t) = -k_s(z_s(t) - z_u(t)) - c(\dot{z}_s(t) - \dot{z}_u(t)) \quad (1)$$

$$m_u\ddot{z}_u(t) = k_s(z_s(t) - z_u(t)) - k_u(z_u(t) - z_r(t)) + c(\dot{z}_s(t) - \dot{z}_u(t)) \quad (2)$$

while the same equations can be rewritten as

$$m_s\ddot{z}_s(t) = -k_s(z_s(t) - z_u(t)) + f(t) \quad (3)$$

$$m_u\ddot{z}_u(t) = k_s(z_s(t) - z_u(t)) - k_u(z_u(t) - z_r(t)) - f(t) \quad (4)$$

when the regenerative set-up is considered. In the above equations, m_s and m_u denote, respectively, the sprung and unsprung masses, z_s and z_u their positions and z_r the road profile. In the passive set-up, the term c denotes the viscous coefficient of the damper and $f(t)$ the force provided by the electromagnetic actuator while, in both set-ups, k_s and k_u denote respectively the suspension and the tyre stiffness. Finally, the quantity $z_s - z_u$ represents the suspension stroke and $z_u - z_r$ the tire deflection.

Note that, being the damper a dissipative device, it has been removed in the regenerative set-up considered here because the aim is that of maximising the harvestable energy. A force generator is used in its place to dampen the vertical motion and transform such energy in electrical power.

1.2 Electromechanical actuator model

In this paper, for simplicity, we consider a linear permanent-magnets electromechanical motor as force actuator (LPMA). The LPMA solution is preferable because the employment of magnets permits to avoid the excitation circuit that needs power for it to work. An alternative solution may be that of using a rotary electrical motor with a mechanical transmission for motion's conversion. However, this kind of solution has usually a lower efficiency because of the high friction's losses. The linear dynamic equations of a generic LPMA actuator (Jang, Choi, Cho, & Lee, 2005) are given by

$$v_a(t) = R_a i(t) + L_a\frac{di(t)}{dt} + K_v v(t) \quad (5)$$

$$f(t) = K_v i(t) \quad (6)$$

where f is the damping force, i the armature current, v_a the armature voltage and v the compression rate (vertical speed of the suspension stroke). The parameters R_a and L_a represent, respectively the armature resistance and inductance while K_v is the force constant. It is very important to choose the parameters in such a way that the electrical power flowing through the machine is characterised by high voltages and low currents in order to have little Joule losses and, in turn, a good efficiency. A way to achieve this is to choose, compatibly to other physical realisation constraints, actuators with high values for the force constant K_v and low values for R_a. Other kinds of losses are less important and are here neglected for simplicity.

1.3 Overall control architecture

In Figure 2, the overall control architecture is presented which consists of two nested control loops (*Cascade Control*), governed respectively by the *Current Controller* (CC) and the *Regenerative Vibration Controller* (RVC). CC is the internal controller of the four-quadrant DC–DC converter aimed at regulating the armature current loop so as to establish the correct bidirectional electrical power flows between the energy storage (battery) and the actuator. The circuital representation of the DC–DC converter is depicted in Figure 3. It is characterised by the following quantities:

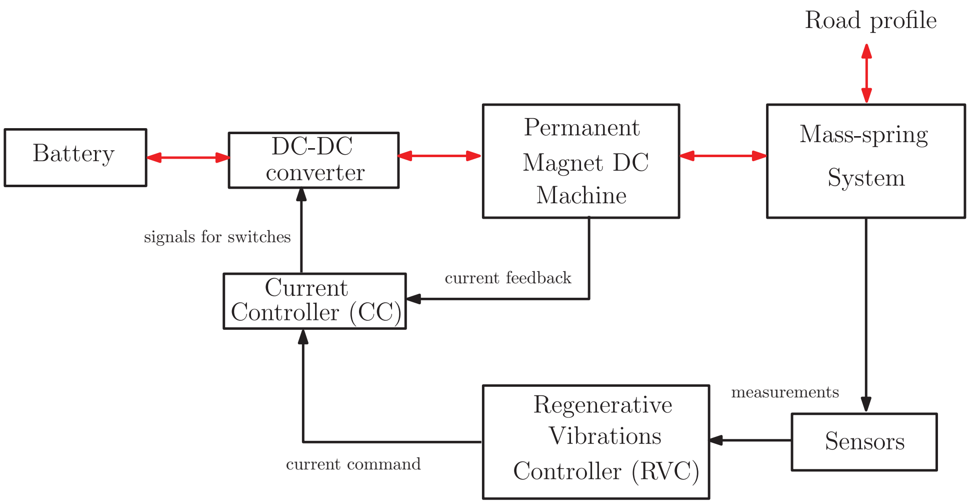

Figure 2. Overall control architecture.

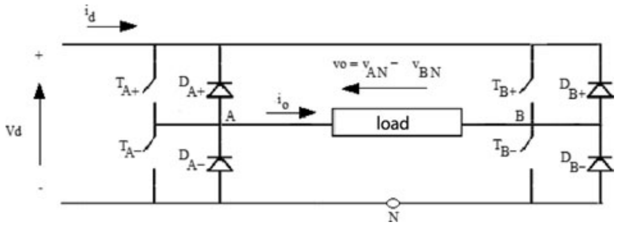

Figure 3. DC–DC converter circuit.

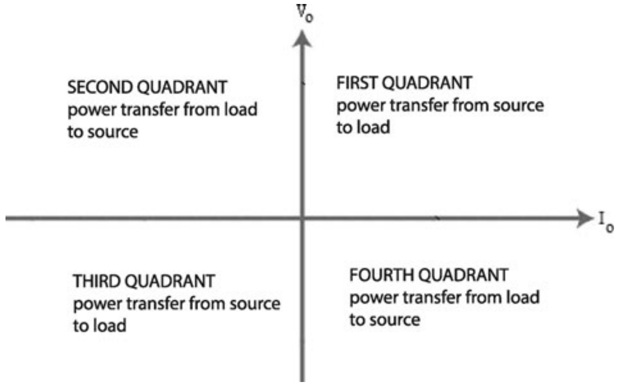
V_o
SECOND QUADRANT
power transfer from load to source
FIRST QUADRANT
power transfer from source to load
I_o
THIRD QUADRANT
power transfer from source to load
FOURTH QUADRANT
power transfer from load to source

Figure 4. Four-quadrant characteristic for the DC–DC converter.

- v_d: input dc voltage;
- i_d: input dc current;
- v_o: output voltage whose amplitude and sign can be controlled;
- i_o: output current;
- $T_{A+}, T_{B+}, T_{A-}, T_{B-}$: controlled switches;
- $D_{A+}, D_{B+}, D_{A-}, D_{B-}$: diodes;
- *load*: electromagnetic motor.

and behaves according to the four quadrants chart depicted in Figure 4.

The CC block consists of a PI control law which is used to maintain the armature current at suitable reference values provided by the outer RVC controller. The related control signals conveyed to the DC–DC converter are modulated via a PWM. Its design however is not considered here for brevity. Moreover, being its time constants expected to be remarkably smaller than that of the RVC loop, the inner current loop dynamics can be neglected during the RVC design. Then, hereafter we focus on the control design problem underlying the synthesis of the RVC controller which is expected to provide the usual control performance of standard active suspension systems plus the ability to harvest as much energy as possible.

2. Control design specifications and power flow analysis

In classical active and semi-active control design problems, three main design specifications are usually considered: *ride quality*, *road handling* and *suspension stroke*.

The *ride quality* is fundamental requirement for passengers' comfort and is mainly related to the sprung mass acceleration $\ddot{z}_s$. A good suspension system has to maintain this quantity within suitable limits at those frequencies where the human body is more sensitive to mechanical vibrations. For comfort evaluation the ISO-2631 (ISO, 1997) standard may be considered, where an index is proposed that gives a measure of passengers' perception of vibrations: the *ride index* (RI)

$$ride\ \ index := \sqrt{a_x^2 + a_y^2 + a_z^2}, \qquad (7)$$

with

$$a_i(T) = \sqrt{\frac{1}{T}\int_0^T a_{wi}^2(t)dt} \quad i = x, y, z \tag{8}$$

where a_{wi} is the acceleration along the ith axis weighed by the following filter:

$$W(s) = \frac{81.89s^3 + 796.6s^2 2 + 1937s + 0.14}{s^4 + 80s^3 + 2264s^2 + 7172s + 21196} \tag{9}$$

The norm provides the above filter because it weights the frequencies whom the human body is particularly sensitive to. Note that lower values of the ride index imply better vibrations' attenuation. In the present application, because only the vertical acceleration is of interest, the ride index essentially coincides with a_z. *Road handling* is an another important objective and it is mainly related to vehicle and passengers' safety. It becomes extremely important in sportive or race cars. It is usually represented by the tyre deflection $z_u - z_r$ while the *suspension stroke* is usually represented by $z_s - z_u$. Obviously, suitable norms of the above control objectives are to be minimised for optimising the corresponding performance.

A regenerative suspension system has of course to take into account all the above specifications for its design. However, an additional requirement on the amount of electrical harvested energy has to be considered too. To this end, relevant variables are the electrical power P_e and the mechanical power P_m of the electrical motor, defined as

$$P_e(t) = \eta P_m(t) \tag{10}$$

$$P_m(t) = f(t)\,(\dot{z}_s(t) - \dot{z}_u(t)) \tag{11}$$

when the motor acts as a generator (that is $P_m(t) < 0$), $P_e(t)$ is the useful power that can potentially be harvested. Note that $P_e(t)$ is a fraction of P_m, with η the corresponding conversion efficiency. On the contrary, when $P_m(t) > 0$, the electromagnetic actuator acts as a motor and the electrical power $P_e(t)$ is spent to produce the mechanical power $P_m(t)$. Finally, the power dissipated by the Joule effect can be expressed as

$$P_d(t) = R_a i^2(t) \tag{12}$$

and motives the need of using high voltages and low currents in this kind of applications.

2.1 *Power flows analysis*

In order to arrive to consistent guidelines on how to maximise the harvestable electrical energy, a power flows analysis of the regenerative suspension system is accomplished in this subsection. From a systemic viewpoint, the latter can be considered as a series of two-port subsystems, as depicted in Figure 5 – with the dual variables on each terminal indicated between parenthesis – where P_s, acting at the input terminal of the first subsystem, represents the power exchanged with the road:

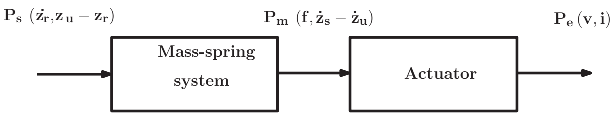
$P_s\ (\dot{z}_r, z_u - z_r)$
$P_m\ (f, \dot{z}_s - \dot{z}_u)$
$P_e\ (v, i)$
Mass-spring system
Actuator

Figure 5. Power flows.

$$P_s(t) := -k_u \dot{z}_r(t)(z_u(t) - z_r(t)) \tag{13}$$

In all terminals of the two-port system we adopt the convention that the power is entering into the system when positive.

With reference to Figure 1, it is easy to understand that the road profile z_r is the only exogenous signal in the system that excites the suspension and it is the only source of power to be harvested. In the forthcoming analysis, vehicle's pitch and roll motions will not be considered for simplicity. Then, in the above simplified driving scenario no energy can be harvested on flat roads ($\dot{z}_r = 0$). In order to exactly quantify the power flows we have to consider the total mechanical energy stored into the system, given by the sum of the kinetic energy of the masses and the potential energy of the springs:

$$\begin{aligned} E(t) = {} & \frac{1}{2}m_s\dot{z}_s^2(t) + \frac{1}{2}m_u\dot{z}_u^2(t) + \frac{1}{2}k_s(z_s(t) - z_u(t))^2 \\ & + \frac{1}{2}k_u(z_u(t) - z_r(t))^2 \end{aligned} \tag{14}$$

Because we do not make use of dissipative devices like viscous shock-absorbers, the only way the power is exchanged and may be dissipated is through the road and actuator terminals. The road irregularities can introduce energy or can absorb the potential energy stored in the springs when they discharge. Similarly, the actuator can absorb part of the energy stored in the system when it acts as a generator or can introduce energy into the system taking it from the battery when acts as a motor.

Then, we can write the following instantaneous power balance:

$$\dot{E}(t) = P_s(t) + P_m(t) \tag{15}$$

where $\dot{E}(t)$ represents the instantaneous power stored into the system. By expanding expression (14) it is found

$$\begin{aligned}\dot{E}(t) = m_s\dot{z}_s(t)\ddot{z}_s(t) + k_s(\dot{z}_s(t) - \dot{z}_u(t))(z_s(t) - z_u(t))\\ + m_u\dot{z}_u(t)\ddot{z}_u(t)\\ + k_u(\dot{z}_u(t) - \dot{z}_r(t))(z_u(t) - z_r(t))\end{aligned} \tag{16}$$

and, by using the system dynamics (1) and (2), after direct manipulations one arrives to

$$\dot{E}(t) = f(t)(\dot{z}_s(t) - \dot{z}_u(t)) - k_u\dot{z}_r(t)(z_u(t) - z_r(t)) \tag{17}$$

By direct examination, it follows that the first-term is related to the actuator whereas the second is related to the road. The above expressions related to P_m and P_s allow one to draw out several considerations:

(1) An ideal control design would consist of having both quantities sign-defined for all time. In particular, one would like

$$P_m(t) << 0, \quad P_s(t) >> 0 \text{ and } P_m(t) = -P_s(t), \tag{18}$$

conditions (18) would ensure that P_s is large and always flowing from the road to the suspension system whereas P_m is large as well and always flowing from the suspension to the battery. This means that all the power induced by road irregularities is harvested. In addition, condition $P_m(t) = -P_s(t)$ would imply also that $\dot{E}(t) = 0$ which would ensure that the system has a perfect transfer of energy. However, in practical situations, only approximations of the above favourable control scenario are realistic.

(2) Because $f(t)$ is a directly manipulable variable, it is quite easy to make $P_m(t) < 0$ sign-defined. However, this choice is usually not convenient for harvesting a remarkable amount of energy because it does not take into account the role of P_s into the play. In fact, in the favourable situations whereby $P_m(t) \leq 0$ and $P_s(t) \geq 0$, one arrives easily to the conclusion that the following condition

$$\int_0^T |P_m(t)|dt \leq \int_0^T P_s(t)dt \tag{19}$$

cannot be violated. In fact, Equation (19) results by taking the integral on any interval $[0, T]$ of both sides of Equation (15) and considering that $E(t) \geq 0$ for all t ($E(0) = 0$). Thus, it establishes a bound on the amount of electrical energy $P_e = \eta P_m$ that can be harvested and suggests that it might make nonsense to synthesise control strategies that try to maximise P_m if P_s is small and there is no way to increase its amount any further.

(3) As far as P_s is concerned, expression (13) rises several considerations. First of all, observe that P_s is zero either when the road is completely flat ($\dot{z}_r = 0$) or when the tyre deflection is zero, ($z_u(t) - z_r(t) = 0$). While the first condition on the road flatness is quite intuitive the second is somewhat unexpected and puts a trade-off between the harvestable energy and road handling performance. A further consideration is that P_s depends on the regulated variable z_u. Thus, if P_s were made sign-defined and as large as possible, viz. $P_s > >0$, the harvested energy could be increased via a suitable control law regardless of the behaviour (the sign) of P_m, that in this case need not be sign-defined (any active control law could be used). In fact, $P_s > 0$ would provide a barrier for the internal potential energy of the suspension from flowing back towards the road. Then, even if some amount of energy would be provided by the actuator in some circumstances, this amount never would be lost because the system would result to be conservative. These considerations are at the basis of the maximum induced power control (MIPC) design approach that will be presented in the next section and provides the main result of the paper.

3. The maximum induced power control (MIPC) approach

Based on the above considerations, it could be convenient to optimise P_s by making it sign-defined and as large as desired. A rather simple heuristic will be presented hereafter which provides the basic idea of the approach. Consider expression (13). Then, P_s could be made sign-defined ($P_s > 0$) if did exist a suitable control law able to enforce the following model reference condition

$$z_u(t) - z_r(t) = -\alpha\dot{z}_r(t) \tag{20}$$

in closed-loop, where α is a scalar design parameter. If Equation (20) were true at each time instant the induced power would become

$$P_s(t) = k_u\alpha\dot{z}_r^2(t) \tag{21}$$

Therefore, the power coming from the road always would flow into the system and could be made as large as required by choosing suitable values for α. Obviously, it is not possible to make α arbitrarily large for having an arbitrarily large harvest energy. In fact, this would increase the current $i(t)$ and over a certain threshold the Joule effect would reduce the harvested energy instead of increasing it. In that case, P_s would increase at the expenses of the energy taken from the battery. The designer has to tune this parameter by increasing it until a convenient amount of harvested energy is achieved.

Condition (20) provides a control design objective for energy harvesting maximisation. However, when the other, possibly conflicting, usual control objectives have to be considered the next problem is how to recast all of them in the same control design framework. To this end, because the $\mathcal{H}_\infty$ control design approach has been largely considered in active and semi-active suspension control design problems we focus hereafter with this control strategy and it will be shown how the energy harvesting objective can be converted in the $\mathcal{H}_\infty$-norm minimisation of a suitable causal transfer function. To this end, let us introduce the following performance output z_p

$$z_p(t) = z_u(t) - z_r(t) + \alpha \dot{z}_r(t) \tag{22}$$

and observe that $z_p(t) = 0$ implies that the condition (20) holds true. Then, if a causal closed-loop transfer function between z_r and z_p did exist, say (with a little abuse of notation) $z_p = W_{z_p,z_r}(s)z_r$, the energy/power of z_p could be minimised by minimising the $\mathcal{H}_\infty$-norm of $W_{z_p,z_r}(s)$ provided that z_r is in a specific class of signals with finite energy/power. Note also that, because both z_r and $\dot{z}_r$ appear in Equation (22), a causal transfer function W between z_r and z_p does not exist in general. On the contrary, it always exists when $\dot{z}_r$ is used as the exogenous signal instead of z_r, that is $z_p = W_{z_p,\dot{z}_r}(s)\dot{z}_r$. Thus, in the next section a suitable state-space formulation will be described and the overall multiobjective $\mathcal{H}_\infty$ control design problem fully detailed.

Finally, it is convenient to consider α as a stable filter rather than a scalar: this allows one to have system representations not in descriptor form, as they on the contrary would result by the use of a pure constant K_f, and to have the energy harvesting prescription expressible as linear combination of states, as required by the LMI control design method used here:

$$z_p = z_u - z_r + \alpha(s)\dot{z}_r \tag{23}$$

A simple first-order filter

$$\alpha(s) = \frac{K_f}{s\tau + 1} \tag{24}$$

will be considered hereafter for simplicity with only two tuning parameters to be chosen: the gain K_f and the time constant τ. In order the filter behaves practically as a constant, the time constant τ should be chosen of course as small as possible without leading to numerical problems and K_f as large as possible, to improve the energy harvesting performance. Higher order filters might help in achieving better performance but they complicate the control design. The analysis with higher order filters will be undertaken in future studies.

3.1 Multiobjective $\mathcal{H}_\infty$ control design problem

For causally realising z_p in Equation (23) is necessary to work with a system description which takes into account as exogenous signal the derivative $\dot{z}_r$ instead of z_r. To this end, the state-space representation used in Chen and Guo (2005) is considered enlarged to include $\tilde{\dot{z}}_r := \alpha(s)\dot{z}_r$, with $\alpha(s)$ the first-order lag (24). Then, the following state-space representation results

$$\dot{x}(t) = Ax(t) + Bu(t) + E\dot{z}_r(t) \tag{25}$$

with state vector

$$x = \left[\, z_s - z_u \;\; \dot{z}_s \;\; z_u - z_r \;\; \dot{z}_u \;\; \tilde{\dot{z}}_r \,\right]^T \tag{26}$$

and system matrices

$$A = \begin{bmatrix} 0 & 1 & 0 & -1 & 0 \\ -\dfrac{k_s}{m_s} & 0 & 0 & 0 & 0 \\ 0 & 0 & 0 & 1 & 0 \\ \dfrac{k_s}{m_u} & 0 & -\dfrac{k_u}{m_u} & 0 & 0 \\ 0 & 0 & 0 & 0 & -\dfrac{1}{\tau} \end{bmatrix},$$
$$B = \begin{bmatrix} 0 \\ \dfrac{K_v}{m_s} \\ 0 \\ -\dfrac{K_v}{m_u} \\ 0 \end{bmatrix}, \quad E = \begin{bmatrix} 0 \\ 0 \\ -1 \\ 0 \\ \dfrac{K_f}{\tau} \end{bmatrix} \tag{27}$$

Interestingly enough, the energy harvesting objective $z_p(t)$ can now be rewritten as

$$z_p(t) := z_u(t) - z_r(t) + \alpha(s)\dot{z}_r = x_3(t) + x_5(t) \tag{28}$$

The armature current $u(t) = i(t)$ will be used as control command because we can neglect the DC–DC converter dynamics.

According to the $\mathcal{H}_\infty$ control design philosophy, let $z(t)$ denote the vector of objectives to be minimised. As indicated, e.g. in Sammier et al. (2000), one typically includes in $z(t)$ all specifications about ride comfort, road holding and stroke minimisation. Here, for simplicity of exposition, we consider only the ride comfort as standard specification and add the maximisation of energy harvested and Joule's losses minimisation as new requirements. To this end, the following objective vector can be defined

$$z(t) = \left[\ddot{z}_s(t) \; i(t) \; z_u(t) - z_r(t) + \alpha(s)\dot{z}_r(t) \right]^T \tag{29}$$

that can be written as

$$z(t) = Cx(t) + Du(t) + F\dot{z}_r(t) \tag{30}$$

with

$$C = \begin{bmatrix} -\dfrac{k_s}{m_s} & 0\,0\,0\,0 \\ 0 & 0\,0\,0\,0 \\ 0 & 0\,1\,0\,1 \end{bmatrix}, \quad D = \begin{bmatrix} \dfrac{K_v}{m_s} \\ 1 \\ 0 \end{bmatrix}, \quad F = 0_{3\times 1} \tag{31}$$

As also common in the optimal $\mathcal{H}_\infty$ control design approach, it is convenient to filter the objectives. To this end, by denoting $W_u(s)$ a low-pass filter for the current, we consider

$$W_z(s) = \text{diag}\left\{W(s),\; W_u(s),\; 1\right\} \tag{32}$$

as the overall filter for the objective vector z, where $W(s)$ has been already defined in Equation b(9). Also, an input filter $W_d(s)$ is used to shape the energy of the road profile $\dot{z}_r$. Then, by denoting with (A_z, B_z, C_z, D_z) and (A_d, B_d, C_d, D_d) the minimal state-space realisations of $W_z(s)$ and, respectively, $W_d(s)$, the overall augmented plant can be achieved:

$$\begin{cases} \dot{x}_g(t) = A_g x_g(t) + B_{g2}u(t) + B_{g1}\dot{z}_r(t) \\ \tilde{z}(t) = C_{g1}x_g(t) + D_{g12}u(t) + D_{g11}\dot{z}_r(t) \end{cases} \tag{33}$$

where

$$A_g = \begin{bmatrix} A & 0 & EC_d \\ B_zC & A_z & B_zFC_d \\ 0 & 0 & A_d \end{bmatrix}, \quad B_{g1} = \begin{bmatrix} ED_d \\ B_zFD_d \\ B_d \end{bmatrix} \tag{34}$$

$$B_{g2} = \begin{bmatrix} B \\ B_zD \\ 0 \end{bmatrix}, \quad C_{g1} = \left[D_zC \; C_z \; D_zFC_d \right] \tag{35}$$

$$D_{g11} = D_zFD_d, \quad D_{g12} = D_zD \tag{36}$$

Then, by assuming for simplicity the state measurable (or estimable by a suitable observer) a state-feedback controller

$$u(t) = Kx_g(t) \tag{37}$$

can be used. Then, the following closed-loop system results

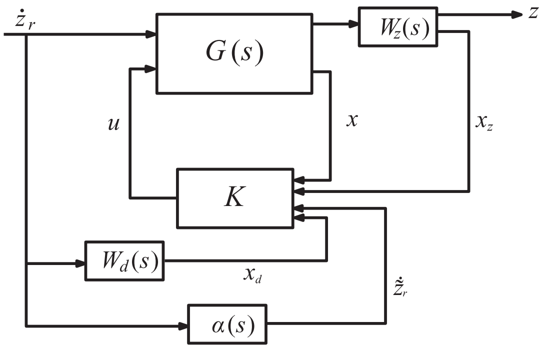

Figure 6. Static state-feedback MIPC control scheme.

$$\begin{cases} \dot{x}_g(t) = (A_g + B_{g2}K)x_g(t) + B_{g1}\dot{z}_r(t) \\ \tilde{z}(t) = (C_{g1} + D_{g12}K)x_g(t) + D_{g11}\dot{z}_r(t) \end{cases} \tag{38}$$

and the control design consists in the minimisation of the $\mathcal{H}_\infty$ -norm of the following transfer matrix:

$$T(s) = (C_{g1} + D_{g12}K)(sI - A_g - B_{g2}K)^{-1}B_{g1} + D_{g11} \tag{39}$$

This can be done, once suitable values for K_f and τ have been selected, e.g. by solving the following LMI programming problem:

$$\begin{cases} \min\limits_{X,Y,\gamma} \gamma \\ \begin{bmatrix} A_{cl} + A_{cl}^T & B_{g1} & (C_{g1}X + D_{12}Y)^T \\ * & -\gamma I & D_{g11}^T \\ * & * & -\gamma I \end{bmatrix} < 0 \\ X = X^T > 0 \\ \gamma > 0 \end{cases} \tag{40}$$

where $A_{cl} := A_gX + B_{g2}Y$ for free matrices $X = X^T > 0$ and Y. If solvable (note that the feasibility of the above optimisation problem depends also on the choice of K_f and τ in Equation (24)), the state-feedback controller is given by $K = YX^{-1}$ and the overall control design scheme is depicted in Figure 6.

3.2 Output feedback implementation

In order to simplify the MIPC implementation, a state observer can be employed to implement the controller. The suspension displacement ($z_s - z_u$) is sufficient to estimate the quarter-car model's states via an observer. Unfortunately, because the derivative of the road profile is also to be used in the MIPC algorithm and one would like to avoid the direct measurement of it, the suspension

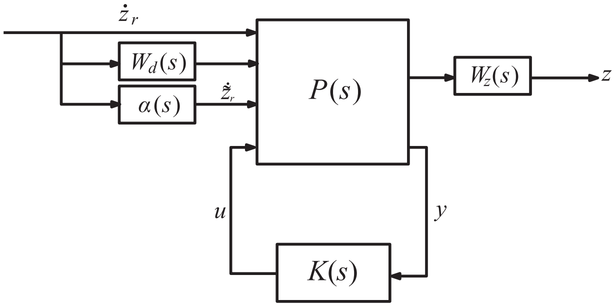

Figure 7. Dynamic output-feedback MIPC control scheme.

displacement measure is not enough informative for its estimation. On the contrary, the latter can be estimated by using additional signals, such as displacements and accelerations. Note also that often such variables are already sensed in current vehicles, with sensors that are quite cheap and light.

In the control literature many techniques have been proposed for real-time road profile estimation, most of them based on sensing the suspension stroke displacement, the sprung mass acceleration and the sprung mass displacement (see e.g. Doumiati, Victorino, Charara, & Lechner, 2011; Imine, Delanne, & M'Sirdi, 2006). These techniques are usually based on the use of a suitable state observers that exploit a dynamic model of the suspension where the road profile and its derivative are included in the state vector. The method adopted here for assessment purposes is borrowed from Scherer, Gahinet, and Chilali (1997) and relies on the design of an output-feedback dynamic controller it is quite simple, being based on the basic quarter-car model, and achieves good performance. The required sensors are the suspension stroke displacement and the sprung mass acceleration: the sprung mass displacement is also a state component of the model but it is estimated through a double integration of the acceleration data. A trapezoidal method is used in Doumiati et al. (2011) for the integration and gives reliable results. The control architecture is depicted in Figure 7 where the plant P has the same structure as in Equation (33) augmented with sensor measurements $y(t) := [z_s(t) - z_u(t), \ddot{z}_s(t)]$. Note the advantage, remarkable for the implementation and control design points of view, that neither $z_r(t)$ nor $\dot{z}_r(t)$ compare directly in $y(t)$:

$$\begin{cases} \dot{x}_g(t) = A_g x_g(t) + B_{g2} u(t) + B_{g1} \dot{z}_r(t) \\ \tilde{z}(t) = C_{g1} x_g(t) + D_{g12} u(t) + D_{g11} \dot{z}_r(t) \\ y(t) = C_{g2}\, x_g(t) + D_{g22}\, u(t) + D_{g21}\, \dot{z}_r(t) \end{cases} \tag{41}$$

where

$$C_{g2} = \left[C_y, \mathbf{0}_{2\times 5}\right], C_y = \begin{bmatrix} 1 & 0 & 0\,0\,0 \\ 0 & -\frac{k_s}{m_s} & 0\,0\,0 \end{bmatrix},$$
$$D_{g21} = [\mathbf{0}_{2\times 1}]\,, D_{g22} = [\mathbf{0}_{2\times 1}]$$

Please note that differently from the previous section, the measurement of the derivative of the road profile is no more needed. The controller will take the following form:

$$K : \begin{cases} \dot{x}_K(t) = A_K\, x_K(t) + B_K\, y(t) \\ u(t) \ \ = C_K\, x_K(t) + D_K\, y(t) \end{cases} \tag{42}$$

with matrices A_K, B_K, C_K, D_K determined by solving the following LMI-based problem:

$$\begin{cases} \min\limits_{X,Y,\hat{A}_K,\hat{B}_K,\hat{C}_K,\hat{D}_K,\gamma} \quad \gamma \\ \begin{bmatrix} R_1^T + R_1 & R_2 & R_3 \\ \star & -\gamma I & (D_{21} + D_{22} D_K D_{11})^T \\ \star & \star & -\gamma I \end{bmatrix} < 0 \\ X = X^T > 0 \\ Y = Y^T \end{cases} \tag{43}$$

where

$$R_1 = \begin{bmatrix} AY + B_{g2}\hat{C}_K & A + \hat{D}_K C_y \\ \hat{A}_K & XA + \hat{B}_K C_y \end{bmatrix},$$
$$R_2 = \begin{bmatrix} B_{g1} + B_{g2}\hat{D}_K D_{g11} \\ XB_{g2} + \hat{B}_K D_{g22} \end{bmatrix},$$
$$R_3 = \begin{bmatrix} C_z Y + D_{g22}\hat{C}_K & C_z Y + D_{g22}\hat{D}_K C_y \end{bmatrix}$$

If the previous optimisation program admits a solution, the matrices of the $\mathcal{H}_\infty$ controller (42) can be obtained as

$$\begin{aligned} D_K &= \hat{D}_K \\ C_K &= \left(\hat{C}_K - D_K C_y Y\right)\left(M^T\right)^{-1} \\ B_K &= N^{-1}\left(\hat{B}_K - XB_u D_K\right) \\ A_K &= N^{-1}\big(\hat{A}_K - N\hat{B}_K C_y Y - XB_u C_K M^T \\ &\quad - X(A + B_u D_K C_y)Y\big)(M^T)^{-1} \end{aligned}$$

where matrices M and N are computed by exploiting the factorisation $NM^T = I - XY$.

4. Simulation results

Several simulations have been performed for testing the effectiveness of the proposed approach. Power spectral

Table 1. (a) Vehicle data and (b) actuator data, from '*Bautzs, Danaher Motion*'. Model: MA508G*.

Parameter	Value
(a)	
Sprung mass	1274 Kg
Front wheels' mass	35.5 Kg
Rear wheels' mass	35.5 Kg
Roll inertia	606.1 Kg · m^2
Pitch inertia	1523 Kg · m^2
Front suspension stiffness	27 kN/m
Rear suspension stiffness	30 kN/m
Front tyre stiffness	228 kN/m
Rear tyre stiffness	228 kN/m
(b)	
Weight	16 Kg
Length	36.5(+20) cm
Force constant	938 N/A
Inductance	5 mH
Resistance	0.05 Ω

*This is an electrical servo actuator model. Retrieved from: http://www.wiki-kollmorgen.eu/wiki/DanMoBilder/file/pdf_archiv/bautz/linearactuators/ma_e.pdf

density of the road's profiles complying with the ISO-8608 standard has been generated and used so as to make the analysis repeatable. The vehicle chosen for the experiments is a standard class-C car, whose parameters are listed in Table 1 together with the actuator's data.

4.1 MIPC control simulations

A output-feedback dynamical MIPC control law was synthesised according to Section 3.2, in three different versions, using three different tunings of the weighting filters and parameters (K_f, τ). In this respect, the YALMIP (Löfberg, 2004) software tool has been used for the complete design of the controllers. The first version (MIPC comfort) has been designed for maintaining the performance very close to those pertaining to a classical passive suspension system with minimal requirements in terms of harvested energy. This first controller corresponds to the choice ($K_f = 13$, $\tau = 0.0005$) where the value of τ has been selected by means of an exhaustive trial-and-error tuning procedure. A second version (MIPC trade-off) has been synthesised with increased requirement in terms of harvested power but with acceptable degradation on the other objectives. This second controller corresponds to the choice ($K_f = 15$, $\tau = 0.0005$). Finally, a third version (MIPC power) has been designed by maximising the harvested power with ($K_f = 18$, $\tau = 0.0005$). This last choice is finalised to drain into the system large amounts of power, more than those that the system can handle without severe performance degradation on the other control specifications. It has to be considered as a limit solution for this system in looking for active control laws that maximise the amount of harvestable power. Note however that higher values for K_f could have been chosen in this example, allowing a further maximisation of the harvestable power.

For comparison purposes, we have also implemented a regenerative damper control law (44), quite simple and common in the literature (Goldner, Zerigian, & Hull, 2001), where the electromagnetic unit is governed in such a way to mimic the behaviour of a passive viscous damper, with the damping parameter c optimised for maximising the harvested energy, $c = 2051.4\ \frac{Ns}{m}$ in this example:

$$i(t) = -\frac{c}{K}\left(\dot{z}_s(t) - \dot{z}_u(t)\right) \tag{44}$$

4.1.1 Frequency behaviour of MIPC

It is very interesting to look at the frequency behaviour of the MIPC controller. Harvestable power is defined by two main variables: $z_u - z_r$ and $\dot{z}_r$. When the phase between these variables is 180°, P_s is positive. For these reasons, the transfer function to be analysed is the one between the derivative of the road profile and the tyre deflection:

$$\frac{Z_u(s) - Z_r(s)}{\dot{Z}_r(s)} \tag{45}$$

which gives an indication of the harvested power contribution at the different frequencies. The Bode plots of the above transfer function for different values of the weighting terms have been depicted in Figure 8 for the RD and MIPC control strategies. In particular, it is possible to observe how the MIPC tuned for trading-off tends to amplify $z_u - z_r$ especially at that frequency where the phase is exactly 180°. Observe also how the response for the comfort-tuned MIPC is quite similar to that of the RD control strategy.

An explanation is that MIPC tends to amplify the magnitude at all frequencies if the maximisation of the harvestable power is the only considered control objective. On the contrary, when also the ride quality is taken into account in the control design, the power is mainly harvested around frequencies where the phases is 180°. In fact, in such a cases only the resonance is amplified.

4.2 Simulations on the quarter-car model

4.2.1 Bump of road

In the first simulation, the quarter-car model has been excited by a 15 × 150 mm bump at a speed of 50 $\frac{\text{km}}{\text{h}}$ depicted in Figure 9. The system responses related to the action of the different controllers are depicted in Figures 10–12. In particular, in Figure 10 the relative suspension deflection is displayed in order to verify that it remains within reasonable suspension limits. The Root Mean Square (RMS) value of the vertical acceleration of the chassis $a_z(t)$ has been reported in order to asses

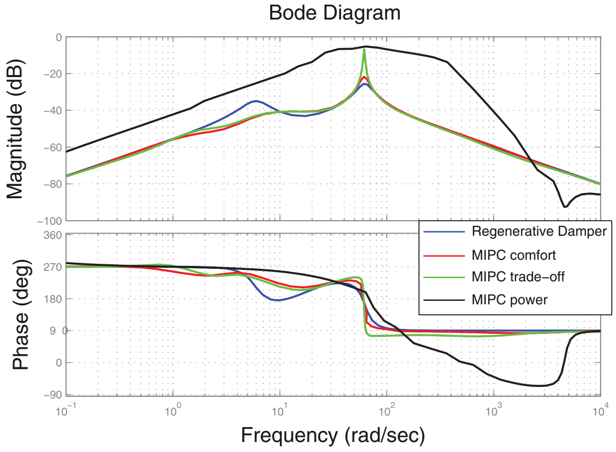

Figure 8. Frequency response of $\frac{Z_u(s)-Z_r(s)}{\dot{Z}_r(s)}$ with MIPC.

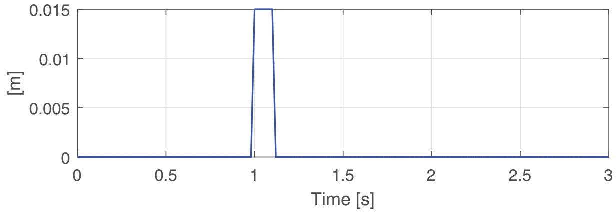

Figure 9. Bump of road of 15 ×150 mm at a speed of 50 $\frac{\text{km}}{\text{h}}$.

the comfort experience during the simulations. Details about the CC in terms of current reference $i(t)$ sent to the current controller CC, control signal and current tracking error, respectively, have been depicted in Figure 11. Finally, in Figure 12 the harvested power for each controller has been reported. It is clear that the MIPC-based scheme is able to gain much more power with respect to the RD approach.

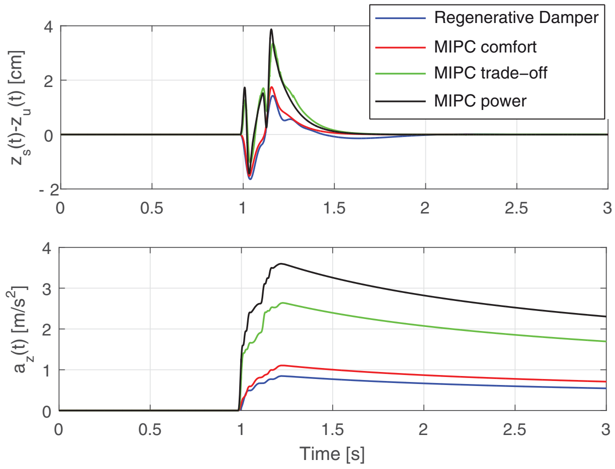

Figure 10. Bump of road test: chassis displacement and vertical acceleration.

4.2.2 Different road classes

Figure 13 has been obtained by Simulink simulations on the quarter-car model (for a single suspension). It depicts in a log scale how the harvested average power changes with the changing of vehicle's longitudinal speed and road roughness. In the picture, three groups of four plots are reported. The three groups correspond to three different road classes (from the below: type A, type C and type D) according to the ISO-8608 standard. Each group of

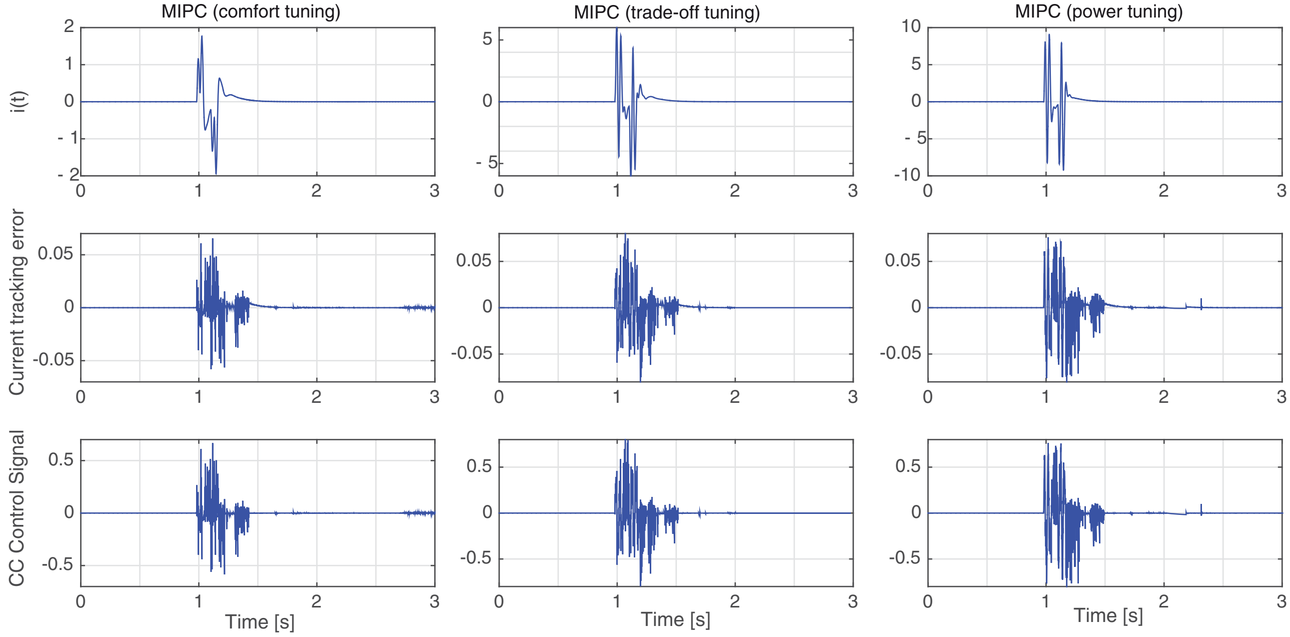

Figure 11. Bump of road test: signals related to the CC.

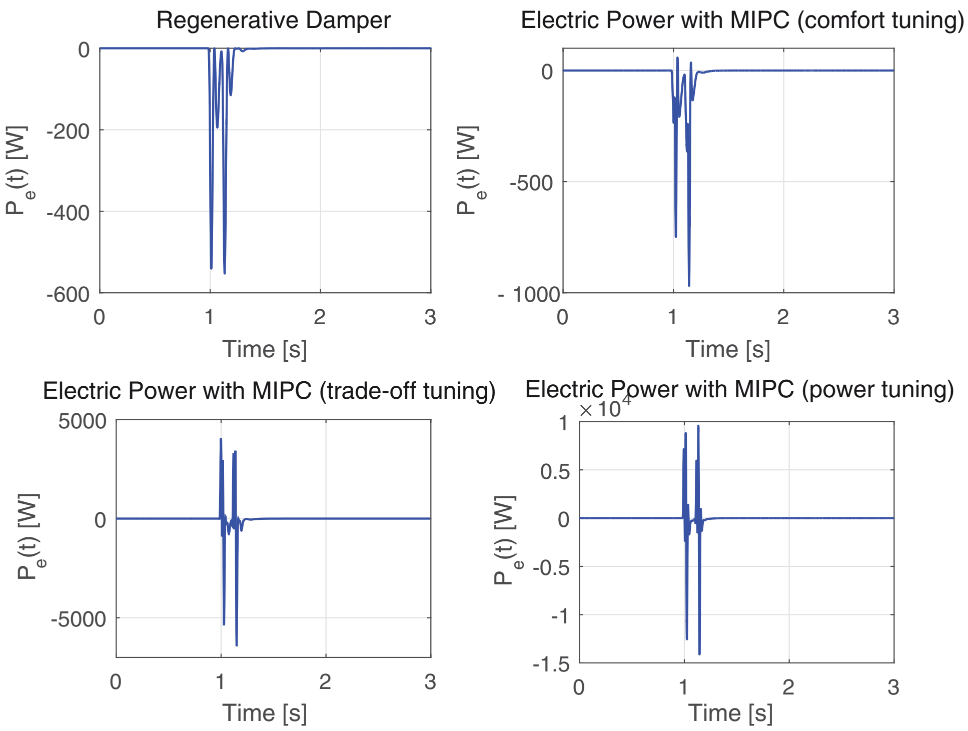

Figure 12. Bump of road test: electrical power under different controllers.

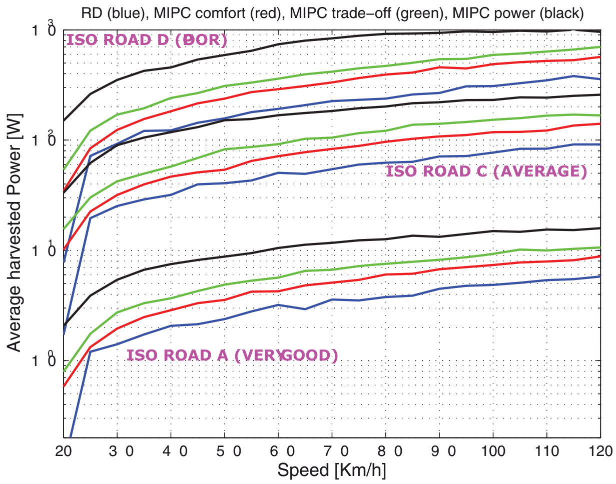

Figure 13. (Colour online) Average power for different controllers and road types versus longitudinal speed.

four plots (RD – blue, MIPC comfort – red, MIPC trade-off – green, MIPC power – black for online version of the paper) reports the average harvested power resulting from driving at constant speed on a straight road under the four controllers.

It is easy to see that there is a remarkable gain in the harvested power by using the proposed MIPC approach with respect to the use of the RD control, the amount of which depending on the tuning of the weighting filters. For example, consider the upper-limit of the C class road for a speed of 50 km/h (typical urban situation): under RD, the average power is about 40 W, while for the three versions of MIPC are 50, 80 and 160 W, respectively. Noticeable enough, this is the harvested power from a single suspension (single wheel).

Finally, plots of the electrical powers generated/consumed by the actuator are reported in Figure 14. Under the passive RD control, the electrical power is always negative as expected: this means that the actuator acts always as a generator and the power flows always from the road to the battery. On the contrary, the active behaviour of the MIPC control law is evident: the power is sometime absorbed and sometime used to correct dynamic behaviour of the suspension system. Furthermore, both the instantaneous peak values (which are not always negative) and the average amount (which is always negative) of the electrical power are higher than in the RD case.

4.3 Simulations on CarSim 8 environment

More detailed simulations were undertaken in the CarSim 8 environment. The controllers were tested on a full (four wheels) vehicle's model, with detailed nonlinear dynamics. Four regenerative suspension systems were used for the four wheels, each one controlled separately (in a decentralised way) by the controller under test. Investigations on the use of a multivariable centralised controller will be undertaken in the future studies.

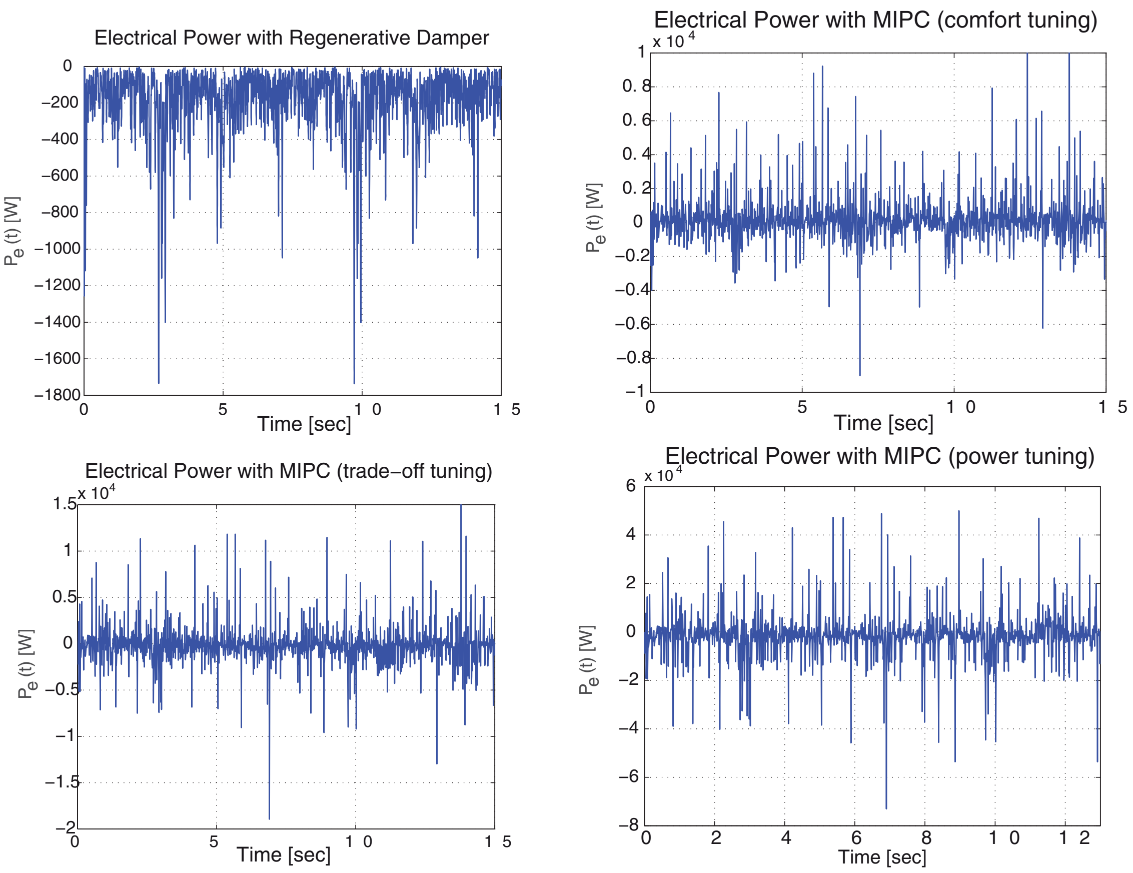

Figure 14. Electrical power under different controllers.

Table 2. Numerical results for tests I and II (four suspensions).

Controller	RI	Max tyre defl.	Av. Elect. Power
[Test I]			
RD	0.55	2.09 cm	190.7 W
MIPC (comfort)	0.65	3.3 cm	265.5 W
MIPC (trade-off)	0.89	4.4 cm	286.5 W
MIPC (power)	2.89	8.5 cm	391.6 W
[Test II]			
RD	0.9	2.63 cm	495.35 W
MIPC (comfort)	1.38	3.5 cm	550.6 W
MIPC (trade-off)	1.53	6 cm	740.8 W
MIPC (power)	2.89	13.8 cm	1233.5 W

Table 3. Numerical results for test III (four suspensions).

	RD	MIPC (comfort)	MIPC (trade-off)	MIPC (power)
Ride index	0.125	0.23	0.25	2.4
Electr. Power [W]	47.1	64.3	65.9	72.6
Max roll [deg]	[−4,3.3]	[−1.9,2.7]	[−1.9,2.7]	[−1.7,2.5]
Max pitch [deg]	[−0.7,2.2]	[−0.02,1.6]	[−0.02,1.7]	[−0.02,1.4]
Max tyre defl. [cm]	1.2	1.97	2.1	2.8

In the first test, the car drives on a straight road with average road roughness (ISO road class C) at 70 km/h while in the second it drives at 18 km/h on a poor road (ISO road class D). Table 2 reports the corresponding values for comparisons and performance evaluation.

In the third and last test, the car drives at 70 km/h on a twisty road with low roughness (ISO road class A). The aim of this simulation is to show how the roll and pitch motions contribute to power generation. This could be of interest even if their motions have not been optimised by the four decentralised controllers. In this respect, Table 3 shows the achieved numerical results.

For the sake of clarity, the videos of these simulations have been published on the web page 'http://t-con-casavola_diiorio_tedesco.kissr.com/'.

In order to analyse the chassis' motions effect on the amount of harvestable energy, it is very useful to look at the plot of the energy versus time corresponding to the use of MIPC with comfort tuning in Figure 15. The constant road roughness's power contribution is depicted by the green line having a constant slope (the slope represents the instantaneous power). During the simulations, some interesting events occur: first, after about two seconds, the car starts cornering a high rolling bend. During this phase, the slope of the blue energy graph increases

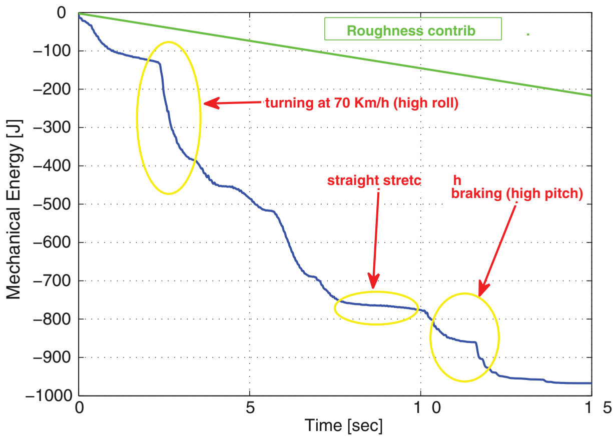

Figure 15. Energy plots on test III (the instantaneous power is represented by the slope of the plots).

Table 4. Power contributions in test III (four suspensions).

Source	Power contribution [W]
Road roughness	14.96 W
Roll (during the first turning)	290.64 W
Pitch (during the braking phase)	76.33 W

remarkably. Between time instants 7 s and 10 s a straight stretch occurs, where only the road roughness contributes to the energy recovery. Finally, around time instant 11 s, the driver claps sharply on the brake and the pitch motion is excited. In this brief time interval, the harvested power increases too.

The average harvested power during the entire simulation is 64.33 W. By evaluating the parts of it at those time intervals when a specific event occurs and by subtracting the constant road roughness contribution, it is possible to make an estimate of how the chassis' motions contribute to power generation (see Table 4).

Remark 4.1: From the above analysis, a consistent amount of energy seems to come from roll and pitching motions. Note that the proposed design framework has not been optimised for maximising the energy harvested during such manoeuvres where the harvesting would be more profitable. For space limitation such a further analysis will be presented elsewhere. It is expected that it can be achieved by redesigning the control strategy on a full-car vehicle model.

Remark 4.2: For comparisons about the ride comfort performance pertaining to the various control laws, please observe that the above tables show the ride index of the RD control strategy. This measure gives a good way of comparisons, because RD behaves like a typical passive system. Note also that the fact that the proposed approach generates less performance on ride comfort compared to passive suspension, even for the comfort case, is a design choice. However, the MIPC method is flexible enough to achieve better ride comfort than RD when required, e.g. in applications where the ride comfort is considered as the first priority and the energy harvesting is just a by-product to achieve if possible. See Casavola, Di Iorio, and Tedesco (2014) for some preliminary results on this class of strategies.

5. Conclusions

The usage of efficient and light regenerative suspension systems can contribute considerably in modern electrical/hybrid cars to their autonomy . The integration of such systems with other existing devices, as regenerative brakes, may help the diffusion of this kind of cars, providing together a total amount of many tens/hundreds watts. This paper has presented an $\mathcal{H}_\infty$-based output feedback scheme for the control of a suspension system in the presence of an electromechanical actuator able to harvest mechanical energy.

An important contribution of this work is the demonstration of the existence of a trade-off between road handling and energy harvesting specifications that limits the design of every kind of regenerative suspension system. It has been also demonstrated that the performance/harvesting trade-off can be dealt with effectively by active control laws as the MIPC here proposed. By classical control techniques, it is possible to design a regulator that achieves classical performance specifications, but it is difficult to act directly on the energy harvesting requirement. The proposed algorithm (MIPC) gives to the designer a way to handle the trade-off in an appropriate manner, depending on the application.

Future works will concern the use of multivariable MIPC control laws designed on the basis of a full four-track model in order to further optimise the performance. Other studies related to the enhancement of the flexibility of the scheme will concern the use form of gain-scheduling MIPC control laws, mostly achieved via fuzzy or LPV control design methods.

Disclosure statement

No potential conflict of interest was reported by the authors.

ORCID

Francesco Tedesco http://orcid.org/0000-0001-5876-3711

References

Casavola, A., & Di Iorio, F. (2012). Increasing energy harvesting in regenerative suspension systems via multiobjective

$\mathcal{H}_\infty$ control. In *Proceedings of the 7th IFAC Symposium on Robust Control Design* (pp. 529–534). Aalborg: IFAC.

Casavola, A., Di Iorio, F., & Tedesco, F. (2014). Gain-scheduling control of electromagnetic regenerative shock absorbers for energy harvesting by road unevenness. In *Proceedings of the American Control Conference* (2114–2119). Portland, OR: IEEE.

Chen, H., & Guo, H.K. (2005). Constrained control of active suspensions: An LMI approach. *IEEE Transactions on Control Systems Technology, 13*(3), 412–421.

Di Iorio, F., & Casavola, A. (2012). A multiobjective $\mathcal{H}_\infty$ control strategy for energy harvesting while damping in regenerative suspension systems. In *Proceedings of the American Control Conference* (pp. 27–29). Montreal: IEEE.

Doumiati, M., Victorino, A., Charara, A., & Lechner, D. (2011). Estimation of road profile for vehicle dynamics motion: Experimental validation. In *Proceedings of the American Control Conference* (pp. 5237–5242). San Francisco, CA: IEEE.

Goldner, R.B., Zerigian, P., & Hull, J.R. (2001). A preliminary study of energy recovery in vehicles by using regenerative magnetic shock absorbers. *SAE Technical Paper Series* (2001-01-2071), Washington, DC.

Imine, H., Delanne, Y., & M'Sirdi, N.K. (2006). Road profile input estimation in vehicle dynamics simulation. *Vehicle System Dynamics, 44*(4), 285–303.

ISO. (1997). International Organization for Standardization *2631-1:1997: Mechanical vibration and shock evaluation of human exposure to whole-body vibration*. Geneva: International Organization for Standardization.

Jang, S.M., Choi, J.Y., Cho, H.-W., & Lee, S.-H. (2005). Dynamic characteristic analysis and experiments of moving-magnet linear actuator with cylindrical halbach array. *IEEE Transactions on Magnetics, 41*(10), 3814–3816.

Löfberg, J. (2004). YALMIP : A toolbox for modeling and optimization in MATLAB. In *Proceedings of the 2004 IEEE International Symposium on Computer Aided Control Systems Design, IEEE, (284–289)*. Taipei.

Montazeri, G.M., & Soleymani, M. (2010). Investigation of the energy regeneration of active suspension system in hybrid electric vehicles. *IEEE Transactions on Industrial Electronics, 57*(3), 918–925.

Pires, L., Smith, M.C., Houghton, N.E., & McMahon, R.A. (2013). Design trade-offs for energy regeneration and control in vehicle suspensions. *International Journal of Control, 86*(11), 2022–2034.

Sabzehgar, R., Maravandi, A., & Moallem, M. (2014). Energy regenerative suspension using an algebraic screw linkage mechanism. *IEEE Transactions on Mechatronics, 19*(4), 1251–1259.

Sagiv Bar, D., & Bobrovsky, B.Z. (2011). Actively controlled vehicle suspension with energy regeneration capabilities. *Vehicle System Dynamics, 49*(6), 833–854.

Sammier, S., Sename, O., & Dugard, D. (2000). $\mathcal{H}_\infty$ control of active vehicle suspensions. In *Proceedings of the IEEE International Conference on Control Applications* (pp. 25-27). Anchorage, AK: IEEE.

Scherer, C., Gahinet, P., & Chilali, M. (1997). Multiobjective output-feedback control via LMI optimization. *IEEE transactions on Automatic Control, 42*(7), 896–911.

Scruggs, J.T. (2010). Multi-objective nonlinear control of semi-active and regenerative systems. In *Proceedings of the American Control Conference* (pp. 726–731). Baltimore, MD: IEEE.

Spelta, C., Previdi, F., Savaresi, S.M., Bolzern, P., Cutini, M., & Bisaglia, C. (2010). A novel control strategy for semi-active suspensions with variable damping and stiffness. In *Proceedings of the American Control Conference* (pp. 4582–4587). Baltimore, MD: IEEE.

Zhang, G., Cao, J., & Yu, F. (2012). Design of active and energy-regenerative controllers for DC-motor-based suspension. *Mechatronics, 22*(8), 1124–1134.

Zuo, L., Scully, B., Shestani, J., & Zhou, Y. (2010). Design and characterization of an electromagnetic energy harvester for vehicle suspensions. *Smart Material and Structures, 19*(4), (1–10).